13

Thruster Modeling and Controller Design for Unmanned Underwater Vehicles (UUVs)

Jinhyun Kim
Seoul National University of Technology
Republic of Korea

1. Introduction

Thruster modeling and control is the core of underwater vehicle control and simulation, because it is the lowest control loop of the system; hence, the system would benefit from accurate and practical modeling of the thrusters. In unmanned underwater vehicles, thrusters are generally propellers driven by electrical motors. Therefore, thrust force is simultaneously affected by motor model, propeller map, and hydrodynamic effects, and besides, there are many other facts to consider (Manen & Ossanen, 1988), which make the modeling procedure difficult. To resolve the difficulties, many thruster models have been proposed.

In the classical analysis of thrust force under steady-state bollard pull conditions, a propeller's steady-state axial thrust (T) is modeled proportionally to the signed square of propeller shaft velocity (Ω),$T=c_1\Omega|\Omega|$ (Newman, 1977). Yoerger et al. (Yoerger et al., 1990) presented a one-state model which also contains motor dynamics. To represent the four-quadrant dynamic response of thrusters, Healey et al. (Healey et al., 1995) developed a two-state model with thin-foil propeller hydrodynamics using sinusoidal lift and drag functions. This model also contains the ambient flow velocity effect, but it was not dealt with thoroughly. In Whitcomb and Yoerger's works (Whitcomb & Yoerger, 1999a; Whitcomb & Yoerger, 1999b), the authors executed an experimental verification and comparison study with previous models, and proposed a model based thrust controller. In the two-state model, lift and drag were considered as sinusoidal functions, however, to increase model match with experimental results, Bachmayer et al. (Bachmayer et al., 2000) changed it to look-up table based non-sinusoidal functions, and presented a lift and drag parameter adaptation algorithm (Bachmayer & Whitcomb, 2003). Blanke et al. (Blanke et al., 2000) proposed a three-state model which also contains vehicle dynamics. Vehicle velocity effect was analyzed using non-dimensional propeller parameters, thrust coefficient and advance ratio. However, in the whole range of the advance ratio, the model does not match experimental results well.

In the former studies, there are three major restrictions. First, thruster dynamics are mostly modeled under the bollard pull condition, which means the effects of vehicle velocity or ambient flow velocity are not considered. However, while the thruster is operating, naturally, the underwater vehicle system is continuously moving or hovering against the current. In addition, the thrust force would be degraded by up to 30% of bollard output due to ambient flow velocity. Therefore, the bollard pull test results are only valid at the

Source: Underwater Vehicles, Book edited by: Alexander V. Inzartsev,
ISBN 978-953-7619-49-7, pp. 582, December 2008, I-Tech, Vienna, Austria

beginning of the operation, and the ambient flow velocity induced by vehicle movement or current must be taken into consideration. Moreover, non-parallel ambient flow effects have received less attention in previous works (Saunders & Nahon, 2002). These are dominant when an underwater vehicle changes its direction, or when an omni-directional underwater vehicle with non-parallel thrusters like ODIN (Choi et al., 1995) is used. Non-parallel ambient flow effects could be modeled simply by multiplying the ambient flow by the cosine function, but experimental results have been inconsistent. Second, in the models including the ambient flow effect, the thrust equations are derived from approximations of empirical results without concern for physical and hydrodynamic analysis. This leads to a lack of consistency in the whole thrust force map, especially, when the directions of thrust force and ambient flow velocity are opposite. Third, most of the previous models contain axial flow velocity of the thruster, because the models are usually based on Bernoulli's equation and momentum conservation. However, measuring axial flow velocity is not feasible in real systems, so we cannot apply those equations directly to the controller. Hence, in Fossen and Blanke's work (Fossen & Blanke, 2000), the authors used an observer and estimator for the axial flow velocity. And, Whitcomb and Yoerger (Whitcomb & Yoerger, 1999b) used the desired axial velocity as an actual axial flow velocity for the thrust controller. Those approaches, however, increase the complexity of controller.

To resolve the above restrictions, in this article, we mainly focus on steady-state response of thrust force considering the effects of ambient flow and its incoming angle, and propose a new thruster model which has three outstanding features that distinguish it from other thruster models. First, we define the axial flow velocity as the linear combination of ambient flow velocity and propeller shaft velocity, which enables us to precisely fit the experimental results with theoretical ones. The definition of axial flow gives a physical relationship between the momentum equation and the non-dimensional representation, which has been widely used to express the relation between ambient flow velocity, propeller shaft velocity, and thrust force. Also, the modeling requires only measurable states, so it is practically feasible. Second, we divide the whole thrust force map into three states according to the advance ratio. The three states, equi-, anti-, and vague directional states, explain the discontinuities of the thrust coefficient in the non-dimensional plot. While the former approaches failed to consider anti- and vague directional states, the proposed model includes all of the flow states. Here, we define the value of border status between anti- and vague directional states as *Critical Advance Ratio (CAR)* where the patterns of streamline change sharply. The details will be given in Section 3. Third, based on the two above features, we develop the incoming angle effects to thrust force. Incoming angle means the angle between ambient flow and thruster, which is easily calculated from vehicle velocity. If the incoming angle is 0 degree, the thrust force coincides with the equi-directional state, or if the angle is 180 degree, the thrust force coincides with the vague or anti-directional state according to the advance ratio. It should be pointed out that the mid-range of incoming angle cannot be described by a simple trigonometric function of advance ratio. So we analyze the characteristics of incoming angle, and divide the whole angle region into the three states above. Also, for the border status among the states, *Critical Incoming Angle (CIA)* is defined.

This chapter is organized as follow: In Section 2, the thruster modeling procedure will be explained and a new model for the thruster is derived. Section 3 addresses three fluid states

with CAR and CIA, and explains the physical meanings. Then Section 4 describes the matching results of experiments with the proposed model simulation, and compares these results with conventional thrust models. Section 5 describes the thruster controller based on the proposed model. Finally, concluding remarks will summarize the results.

2. Basic thruster dynamics model

2.1 Thruster dynamic based on axial flow velocity

The propeller is represented by an actuator disk which creates across the propeller plane a pressure discontinuity of area A_p and axial flow velocity u_p. The pressure drops to p_a just before the disk and rises to p_b just after and returns to free-stream pressure, p_∞, in the far wake. To hold the propeller rigid when it is extracting energy from the fluid, there must be a leftward thrust force T on its support, as shown in Fig. 1.

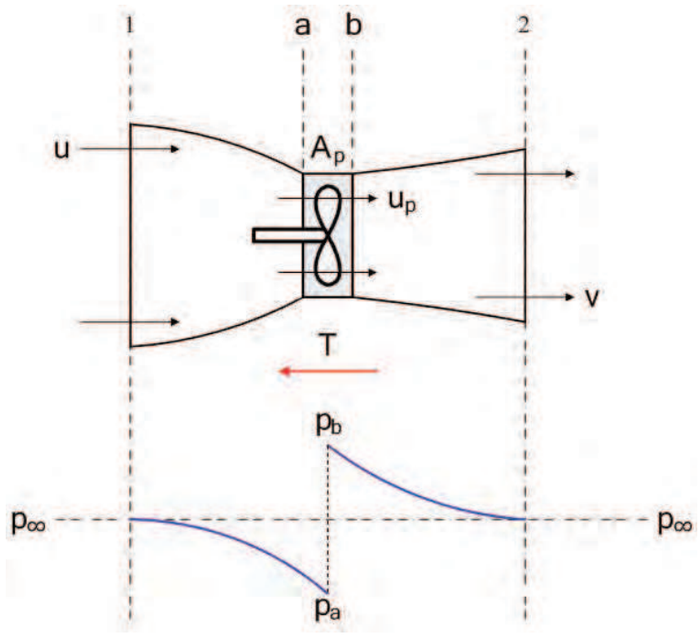

Fig. 1. Propeller race contraction; velocity and pressure changes

If we use the control-volume-horizontal-momentum relation between sections 1 and 2,

$$T = \dot{m}(v - u). \tag{1}$$

A similar relation for a control volume just before and after the disk gives

$$T = A_p(p_b - p_a). \tag{2}$$

Equating these two yields the propeller force

$$T = A_p(p_b - p_a) = \dot{m}(v - u). \tag{3}$$

Assuming ideal flow, the pressures can be found by applying the incompressible Bernoulli relation up to the disk

$$\begin{aligned} \textit{From 1 to a:} \quad & p_\infty + \frac{1}{2}\rho u^2 = p_a + \frac{1}{2}\rho u_p^2, \\ \textit{From b to 2:} \quad & p_\infty + \frac{1}{2}\rho v^2 = p_b + \frac{1}{2}\rho u_p^2. \end{aligned} \tag{4}$$

Subtracting these and noting that $\dot{m} = \rho A_p u_p$ through the propeller, we can substitute for p_b - p_a in Eq. (3) to obtain

$$p_b - p_a = \frac{1}{2}\rho\left(v^2 - u^2\right), \tag{5}$$

or

$$u_p = \frac{1}{2}\left(v + u\right) \Rightarrow v = 2u_p - u. \tag{6}$$

Finally, the thrust force by the disk can be written in terms of u_p and u by combining Eqs. (5) and (6) as follows:

$$T = 2\rho A_p u_p (u_p - u). \tag{7}$$

Up to this point, the procedures are the same as the previous approaches. Now, we define the axial flow velocity as

$$u_p \triangleq k_1 u + k_2 D\Omega, \tag{8}$$

where k_1 and k_2 are constant. The schematic diagram of the axial flow relation is shown in Fig. 2.

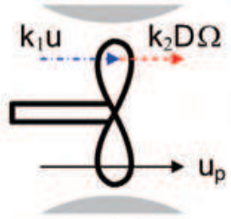

Fig. 2. Proposed axial flow model

For quasi-stationary flow, the axial flow only depends on ambient flow and propeller rotational motion. More complex combinations of ambient flow and propeller velocity are possible, but this linear combination is adequate as will be shown later. This somewhat simplified definition gives lots of advantages and physical meanings.
Finally, substituting Eq. (8) to Eq. (7), the proposed thrust model can be derived as follows:

$$\begin{aligned} T &= 2\rho A_p (k_1 u + k_2 D\Omega)(k_1 u + k_2 D\Omega - u), \\ &= 2\rho A_p (k_1' u^2 + k_2' u D\Omega + k_3' D^2\Omega^2). \end{aligned} \tag{9}$$

This model will be used in the following non-dimensional analysis.

2.2 Non-dimensional analysis

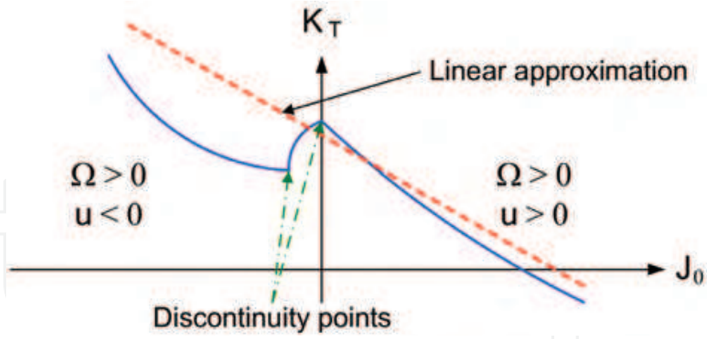

Fig. 3. Thrust coefficient as a function of advance ratio and its linear approximation

The non-dimensional representation for thrust coefficient has been widely used to express the relation between thrust force, propeller shaft velocity and ambient flow velocity as below:

$$K_T(J_0) = \frac{T}{\rho D \Omega |\Omega|}, \tag{10}$$

where $J_0 = u/D\Omega$ is the advance ratio. Figure 3 shows a typical non-dimensional plot found in various references (Manen and Ossanen, 1988; Blanke et al., 2000). In former studies, the non-dimensional relation is only given as an empirical look-up table or simple linear relationship for the whole non-dimensional map as (Fossen & Blanke, 2000).

$$K_T(J_0) = a_1 J_0 + a_2. \tag{11}$$

However, as shown in Fig. 3, Eq. (11) cannot accurately describe the characteristics of the thrust coefficient, especially when $J_0<0$, and, rather than a linear equation, the thrust coefficient seems to be close to a quadratic equation except for the discontinuity points. Even more, Eq. (11) has no physical relationship with thrust force, but is just a linear approximation from the figure.

The proposed axial flow assumption would give a solution for this. The non-dimensionalization of Eq. (9) is expressed as

$$\frac{T}{\rho D^4 \Omega^2} = \frac{\pi}{2}\left[k_1'\left(\frac{u}{D\Omega}\right)^2 + k_2'\left(\frac{u}{D\Omega}\right) + k_3'\right]. \tag{12}$$

And, the quadratic thrust coefficient relation is obtained as following:

$$K_T(J_0) = \frac{\pi}{2}\left[k_1' J_0^{\,2} + k_2' J_0 + k_3'\right]. \tag{13}$$

Hence, contrary to other models, the axial flow definition of Eq. (8) gives an appropriate relationship between the thrust force equation and non-dimensional plot since the derivation was done by physical laws. Also, Eq. (13) can explain the characteristics of the

quadratic equation of the thrust coefficient. From this phenomenon, we can perceive that the axial flow definition in Eq. (8) is reasonable. The coefficients of quadratic equations could be changed depending on hardware characteristics. However, there is still a question of the discontinuities of thrust coefficient in Fig. 3 which has not been answered yet by existing models. This problem will be addressed in the following section.

3. Thrust force with ambient flow model

If ambient flow varies, thrust force changes even with the same propeller shaft velocity, which means that the ambient flow disturbs the flow state under the bollard pull condition. Flow state is determined by a complex relation between propeller shaft velocity, ambient flow velocity and its incoming angle. This will be shown in the following subsections.

3.1 Flow state classification using CAR

In this subsection, we define three different flow states according to the value of advance ratio and the condition of axial flow. To distinguish them, we introduce *Critical Advance Ratio (CAR), J^**.

The three states are as below:

- Equi-directional state

$$J_0 > 0, \tag{14}$$

$$u_p = k_1 u + k_2 D\Omega > 0. \tag{15}$$

- Anti-directional state

$$J^* < J_0 < 0, \tag{16}$$

$$u_p = k_1 u + k_2 D\Omega > 0. \tag{17}$$

- Vague directional state

$$J^* > J_0, \tag{18}$$

$$u_p = k_1 u + k_2 D\Omega < 0. \tag{19}$$

Figure 4 shows the flow states schematically.

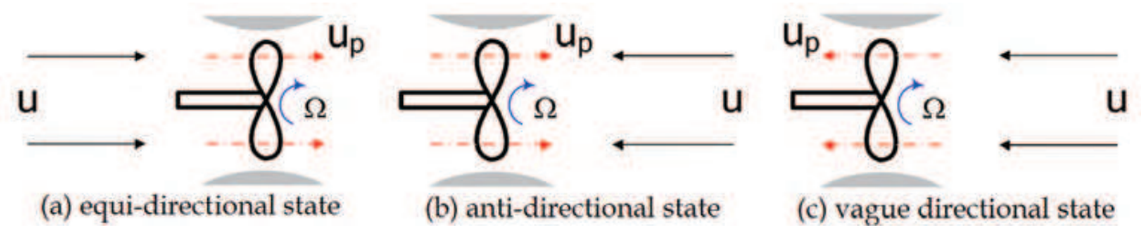

Fig. 4. Three flow states

Equi-directional state: The equi-directional state occurs when the ambient flow direction and axial flow direction coincide. In this state, if the ambient flow velocity increases, the pressure difference decreases. Hence the thrust force reduces, and the streamline evolves as a general form. (Fig. 4(a))
Anti-directional state: The anti-directional state happens when the ambient flow and axial flow direction are opposite. However, the axial flow can thrust out the ambient flow, hence the streamline can be built as sink and source. The Bernoulli equation can be applied and the thrust equation is still valid but the coefficients are different from those of the equi-directional state. Also, the thrust force rises as the ambient flow velocity increases, because the pressure difference increases. (Fig. 4(b))
Vague directional state: In the vague directional state, the axial flow cannot be well defined. The axial flow velocity cannot thrust out the ambient flow; hence the direction of axial flow is not obvious. This ambiguous motion disturbs the flow, so the thrust force reduces. In this case, we cannot guess the form of the streamline, so the thrust relation cannot be applied. However, the experimental results show the proposed thrust relation is still valid in this state. (Fig. 4(c))

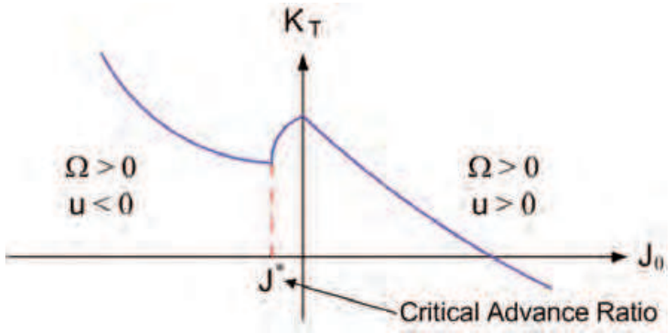

Fig. 5. Thrust coefficient as a function of advance ratio and Critical Advance Ratio (CAR)

Former studies did not consider the anti- and vague directional states, however they can be observed frequently when a vehicle tries to stop or reverse direction. The CAR divides between the anti- and vague directional states as shown in Fig. 5. It would be one of the important characteristics of a thruster. At this CAR point, the ambient flow and propeller rotational motion are kept in equilibrium. Hence, to increase the efficiency of the thruster in the reverse thrust mode, an advance ratio value larger than the CAR is preferable, as shown in Fig. 6.

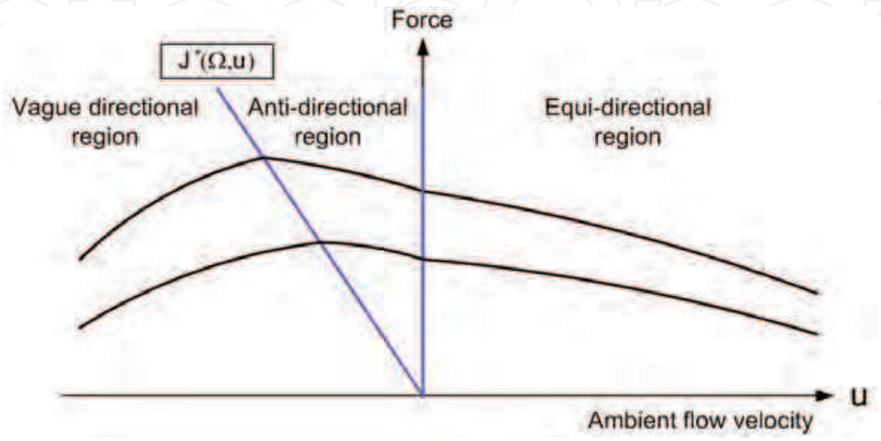

Fig. 6. Thrust force as a function of ambient flow velocity

3.2 Effects of incoming angle on thrust force

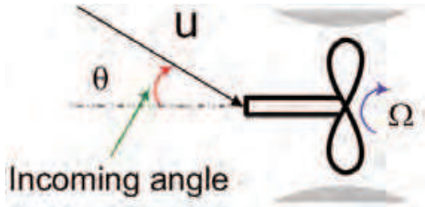

Fig. 7. Incoming angle of ambient flow

In this subsection, the incoming angle effect on thrust force is analyzed. Figure 7 shows the definition of incoming angle. Naturally, if the angle between ambient flow and thrust force is non-parallel, the thrust force varies with the incoming angle. Basically, by multiplying ambient flow velocity by the cosine of the incoming angle, the thrust force can be derived from Eq. (13). In that case, however, the calculated thrust force will not coincide with experimental results except at 0 and 180 degrees, which shows that the incoming angle and ambient flow velocity have another relationship. Hence, we develop the relationship based on experiments, and Fig. 8 shows the result.

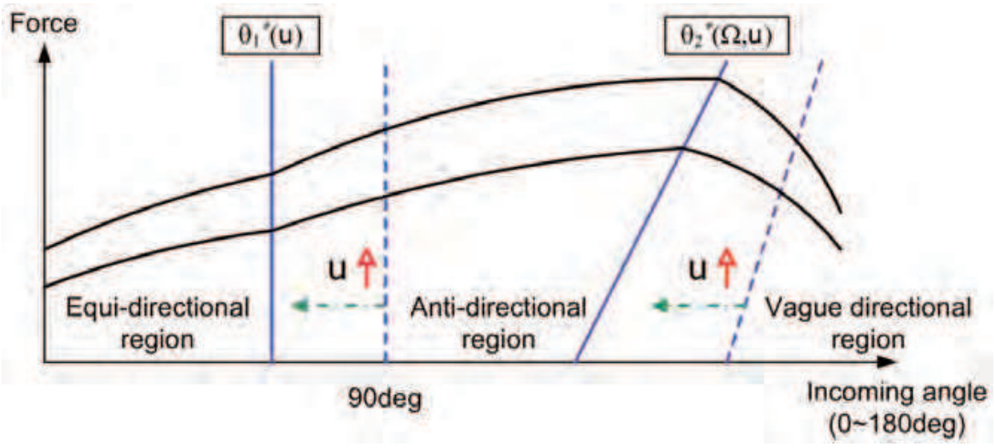

Fig. 8. Thrust force as a function of incoming angle

In Fig. 8, the whole range of angles is also divided into three state regions as denoted in the previous subsection. And, we define the borders of the regions as *Critical Incoming Angles (CIA)* which have the following mathematical relationship.

$$\theta_1^*(u) = \frac{\pi}{2} - a_1 u, \tag{20}$$

$$\theta_2^*(\Omega, u) = a_2 u(\Omega - b_2) + \theta_1^*, \tag{21}$$

where a_1, a_2, b_2, and c_2 are all positive constants. And, $\theta_1^*(u)$ and $\theta_2^*(\Omega, u)$ are the first and second CIA, respectively. Theoretical reasons have not been developed to explain the CIA equations, but empirical results give a physical insight and the above equations can be correlated to experiments. The equi-directional region and anti-directional region are

differentiated with the first CIA. The first CIA only depends on the ambient flow velocity. At the first CIA, the thrust coefficient is the same as the thrust coefficient with no ambient flow velocity. The second CIA separates the anti-directional region and the vague directional region. The second CIA depends not only on ambient flow angle but also on propeller shaft velocity. From Eqs. (20) and (21), the three regions shift to the left as the ambient flow velocity increases.

Now, we derive the incoming angle effect on the thrust force as following:

$$K_T^a = K_T^0 + f_a(J_0, \theta), \tag{22}$$

$$T = K_T^a \rho D^4 \Omega \left|\Omega\right|, \tag{23}$$

where $K_T^0 = K^T(J_0 = 0)$, and

$$f_a = \begin{cases} f_1, & 0 \le \theta \le \theta_1^* \\ f_2, & \theta_1^* \le \theta \le \theta_2^* \\ f_3. & \theta_2^* \le \theta \le \pi \end{cases}; \tag{24}$$

$$\begin{cases} f_1 = (K_T^0 - K_T^+)\left[\sin\left(\dfrac{\theta}{\theta_1^*}\dfrac{\pi}{2}\right) - 1\right] \\ f_2 = K_a J_0 \sin\left(\dfrac{\theta - \theta_1^*}{\pi - \theta_1^*}\dfrac{\pi}{2}\right) \\ f_3 = \left[K_a J_0 \sin\left(\dfrac{\theta_2^* - \theta_1^*}{\pi - \theta_1^*}\dfrac{\pi}{2}\right) - (K_T^- - K_T^0)\right]\cos\left(\dfrac{\theta - \theta_2^*}{\pi - \theta_2^*}\dfrac{\pi}{2}\right) + (K_T^- - K_T^0) \end{cases}$$

In Eq. (22), K_a is a constant which has to be acquired by experiments. $K_T^+ = K_T(J_0)$ and $K_T^- = K_T(-J_0)$. Eq. (22) coincides with Eq. (13) at 0 and 180 degree. Hence Eq. (22) contains all of the effects of ambient flow and implies that the total thrust force is composed of thrust force with bollard pull condition, K_T^0, and additional force induced by ambient flow velocity and its incoming angle, $f_a(J_0, \theta)$.

4. Experimental results

To verify the proposed model, firstly, we operated the thruster under various ambient flow velocities: ±1.2m/s, ±1.0m/s, ±0.8m/s, ±0.6m/s, ±0.4m/s, and 0m/s with a zero degree incoming angle. Then, for 0.4m/s, 0.6m/s and 0.8m/s ambient flow velocities, the thruster was tilted at 5 degree increments from 0 to 180 degree to change incoming angle. For simplicity, we only consider cases where $\Omega > 0$.

In Fig. 9, the experimental thrust forces are compared with simulation results of the proposed model with an input voltage range from 1.5V to 4.5V, which the whole range is between 0.0V and 5.0V for the positive direction. And the range from 0.0V to 0.8V is dead-

zone. Both results are very similar except at some localized points. The deviation could be caused by the thruster not being located in sufficiently deep water due to the restriction of the experimental environment. Thus, the anti- and vague directional response could have been disturbed by spouting water.

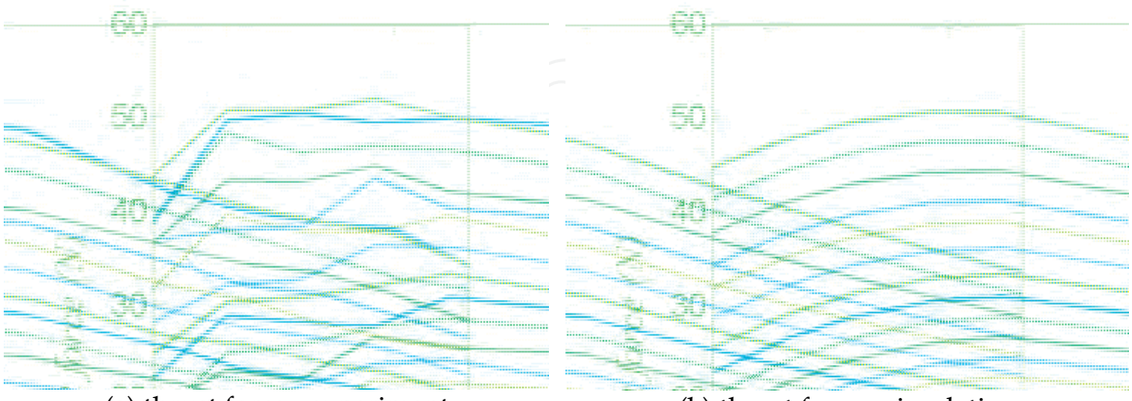

(a) thrust force - experiment (b) thrust force - simulation

Fig. 9. Comparison results of experiment and simulation by the proposed model

To highlight the performance of the proposed model, we compare the results with those of the conventional model described by Eq. (11). The comparison results are shown in Fig. 10. The figure shows that the results of the proposed model are significantly better than the conventional model in the anti- and vague directional regions.

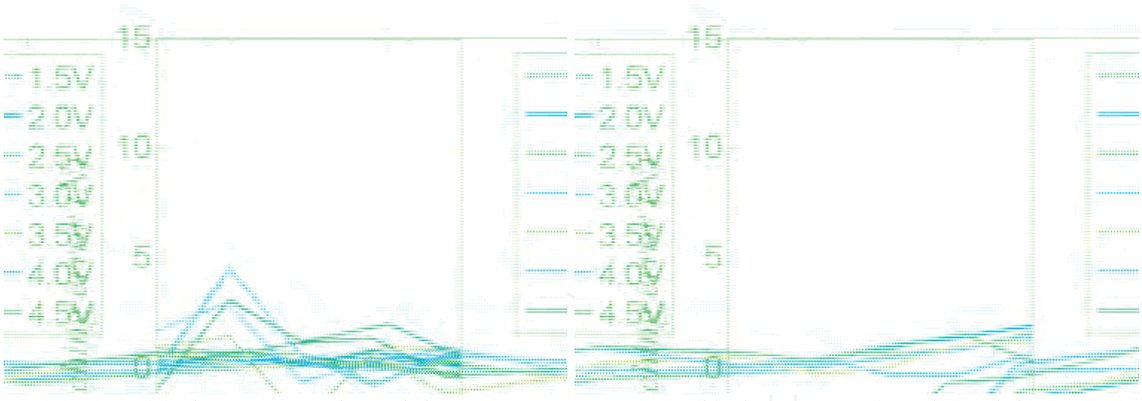

(a) the proposed model (b) the conventional model

Fig. 10. Thrust force matching error

Figures 11(a), 11(c) and 11(e) show the thrust force comparison between experiment and simulation as a function of incoming angle. The errors of matching, as shown in Figs. 11(b), 11(d) and 11(f), are mostly within ±2N. Note that the maximum force of the thrust is up to 50N.

From the matching results with ambient flow velocities and incoming angles, we can say that the initial definition of axial flow is valid, and the proposed model shows good agreement with experimental results under various ambient flow velocities and incoming angles.

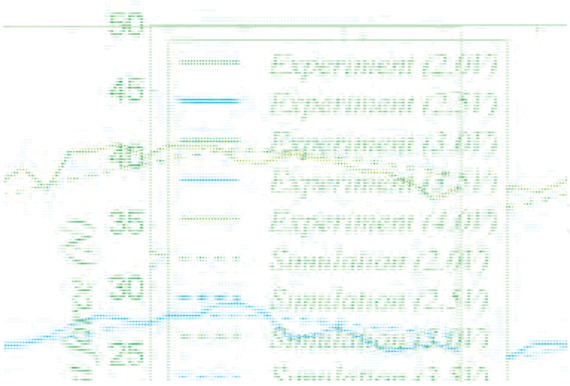

(a) 0.4m/s ambient flow velocity

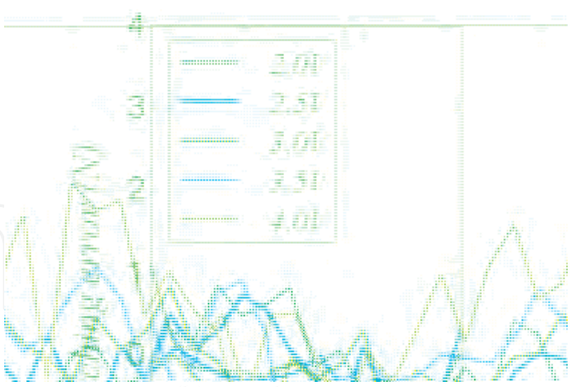

(b) matching error with 0.4m/s ambient flow velocity

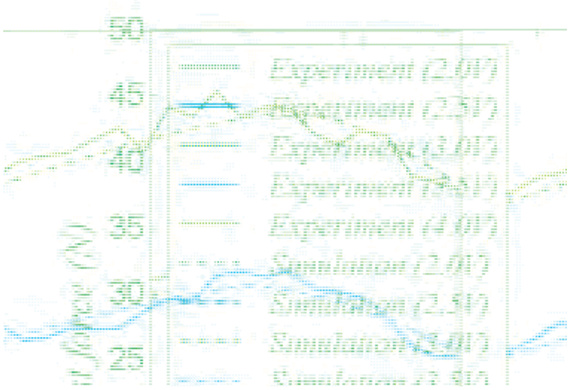

(c) 0.6m/s ambient flow velocity

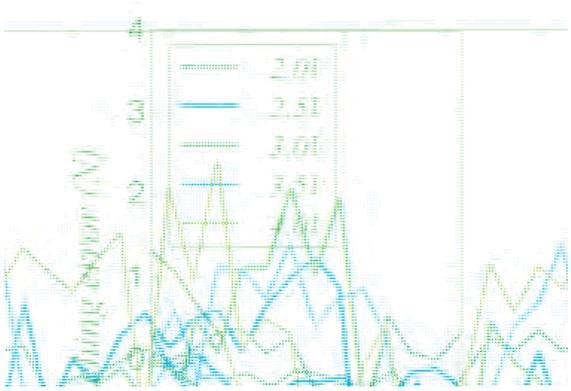

(d) matching error with 0.6m/s ambient flow velocity

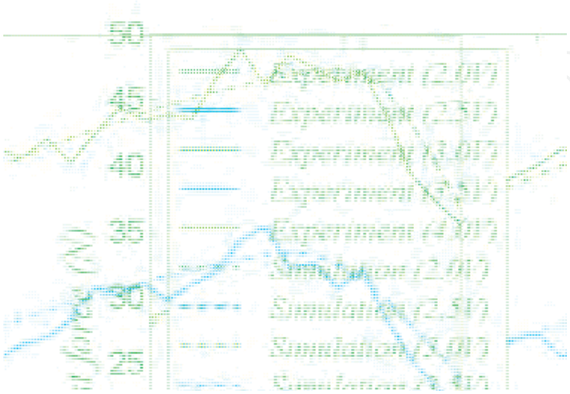

(e) 0.8m/s ambient flow velocity

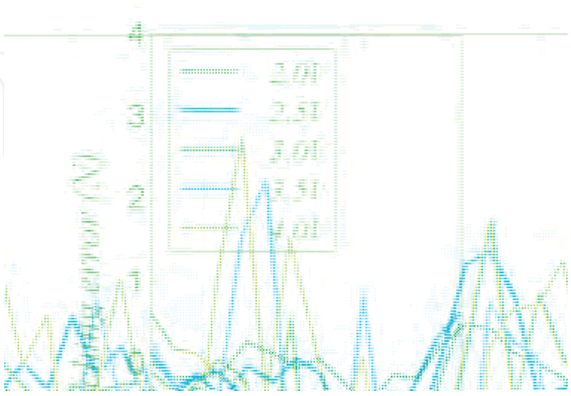

(f) matching error with 0.8m/s ambient flow velocity

Fig. 11. Comparison results of experiment and simulation with incoming angle

5. Thruster controller

5.1 Propeller shaft velocity controller

To obtain the desired thrust force, we need to construct feedback controller with shaft velocity controller. The thruster used in this research only has tachometer for measuring propeller shaft velocity. Hence, firstly, the shaft velocity controller was experimented with open loop and closed loop.

Open Loop (Fig. 12(a))

$$V_{in} = \frac{1}{k_t}(\dot{\Omega}_d + k_{f1}\Omega_d) + \frac{k_{f0}}{k_t}\mathrm{sgn}(\Omega_d) \tag{25}$$

Closed Loop (Fig. 12(b))

$$V_{in} = \frac{1}{k_t}(\dot{\Omega}_{ref} + k_{f1}\Omega) + \frac{k_{f0}}{k_t}\mathrm{sgn}(\Omega) \tag{26}$$

where

$$\dot{\Omega}_{ref} = \dot{\Omega}_d + k_P(\Omega_d - \Omega) + k_I\int(\Omega_d - \Omega) \tag{27}$$

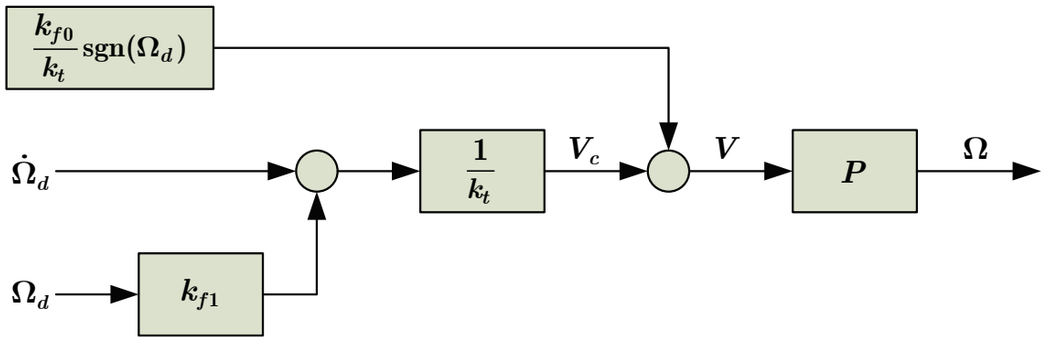

(a) open loop controller

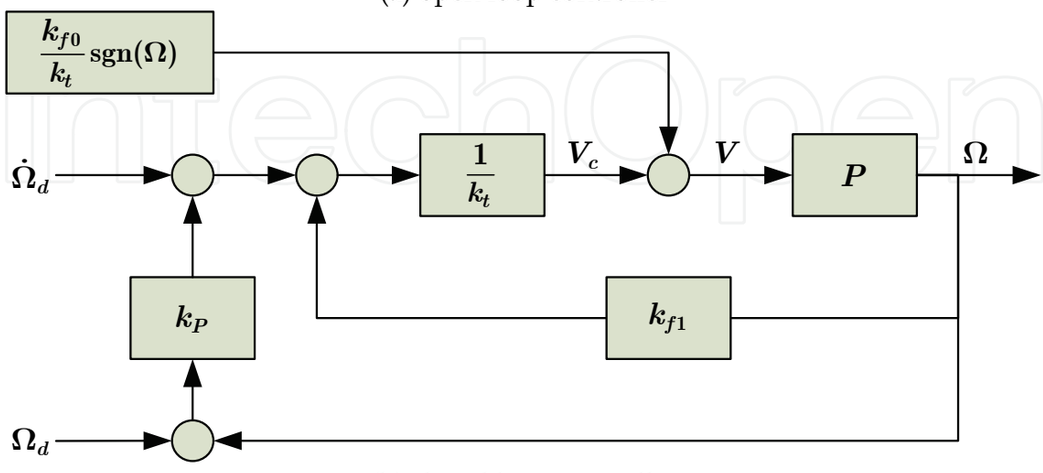

(b) closed loop controller

Fig. 12. Propeller shaft velocity controller

In Fig. 12, P represents the plant model of thruster and V means the final voltage input to the thruster hardware driver.

5.2 Thrust force controller

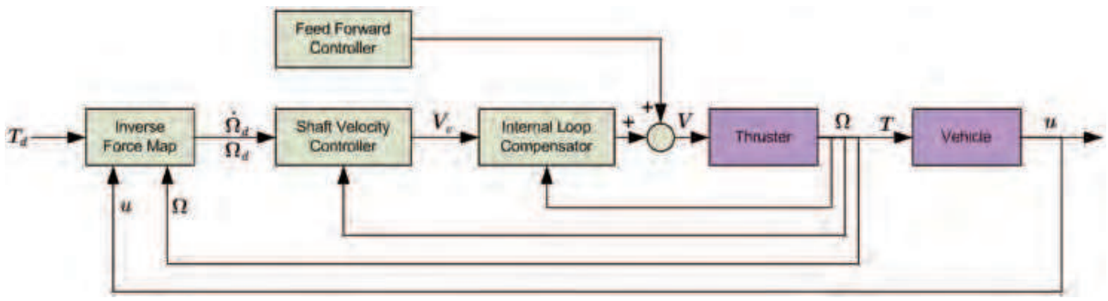

Fig. 13. Diagram of thrust force controller

The overall thrust force controller is composed as Fig. 13. However, the inverse force map only gives the desired shaft velocity according to the desired force. Hence, for the accurate control, the desired shaft acceleration is required. In this chapter, the filtered derivative algorithm is used for the draw of the desired acceleration signal using the desired velocity input.

5.3 Preliminary thruster controller experiments

The Bollard-pull condition was tested with open loop and closed loop controller. The closed loop results (Fig. 14) are normally better than open loop results, but the peak error is larger. This comes from the flexible experimental structure. Hence, if the real systems which dose not have structural flexibility, it is expected that the closed loop performance will be better than open loop performance. As shown in the results, the experimental results are good matching with the model. The force control errors are normally less than 5%.

6. Conclusions

In this chapter, a new model of thrust force is proposed. First, the axial flow as a linear combination of the ambient flow and propeller shaft velocity is defined which are both measurable. In contrast to the previous models, the proposed model does not use the axial flow velocity which cannot be measured in real systems, but only uses measurable states, which shows the practical applicability of the proposed model. The quadratic thrust coefficient relation derived using the definition of the axial flow shows good matching with experimental results.

Next, three states, the equi-, anti-, and vague directional states, are defined according to advance ratio and axial flow state. The discontinuities of the thrust coefficient in the non-dimensional plot can be explained by those states. Although they have not been treated previous to this study, the anti- and vague directional states occur frequently when a vehicle stops or reverses direction. The anti- and vague directional states are classified by CAR (Critical Advance Ratio), which can be used to tune the efficiency of the thruster.

Finally, the incoming angle effects to the thrust force, which are dominant in turning motions or for omni-directional underwater vehicles, are analyzed and CIA (Critical Incoming Angle) was used to define equi-, anti-, and vague directional regions.

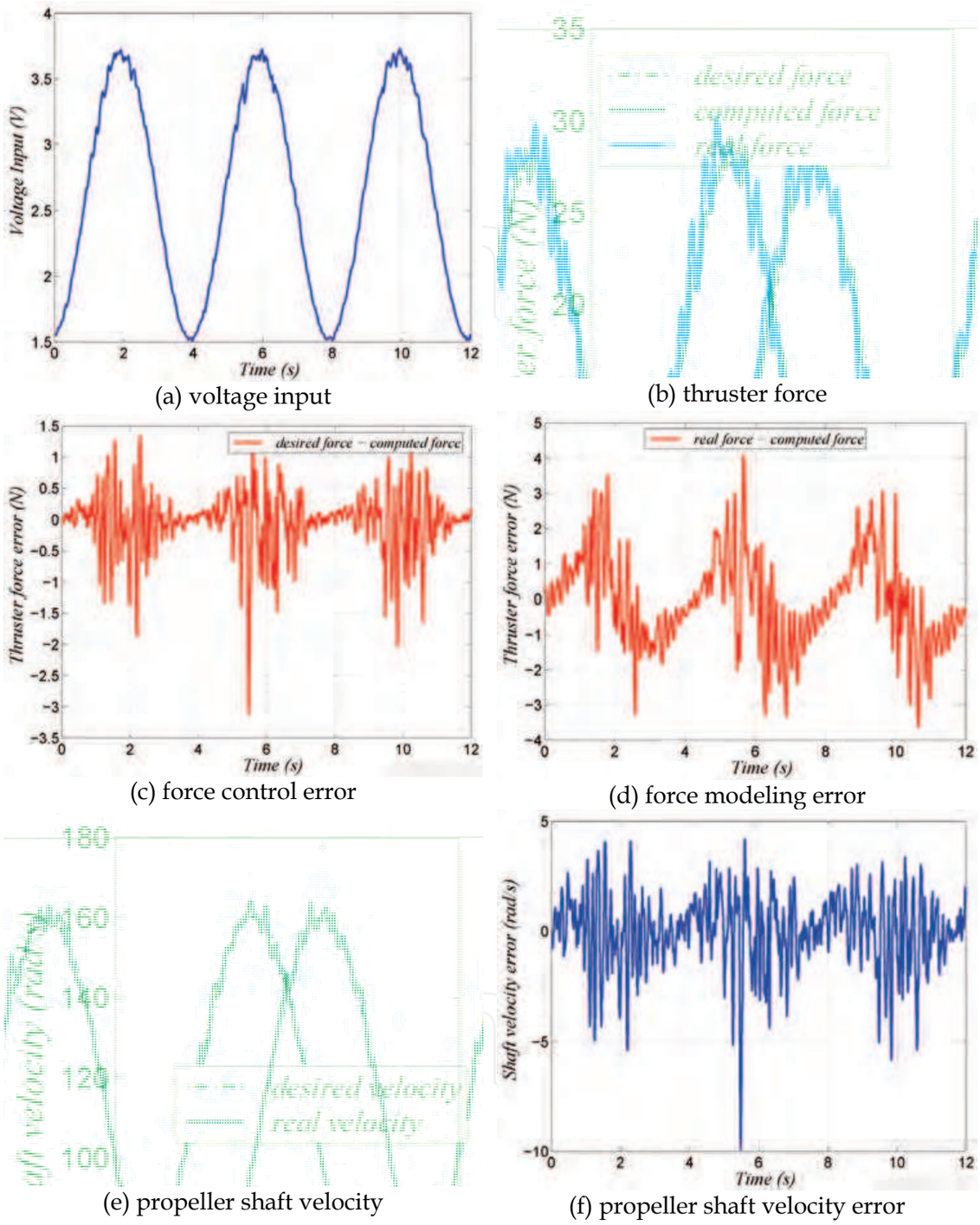

(a) voltage input (b) thruster force

(c) force control error (d) force modeling error

(e) propeller shaft velocity (f) propeller shaft velocity error

Fig. 14. Experimental thruster control performance of closed loop

The matching results between simulation with experimental results show excellent correlation with only ±2N error in the entire space of thrust force under various ambient flow velocities and incoming angles. Note that the maximum force of the thrust is up to 50N. The results are also compared with conventional thrust models, and the matching

performance with the proposed model is several times better than those of conventional linear ones.

Also in this article, the thrust force control performance of the proposed thruster model was examined. From the results in section 5, the best performance can be obtained by the open loop control with accurate model, because the thrust force cannot be measured directly. This means the force map from the propeller shaft velocity to thrust force plays important roll in control performance. The control performance with the model is acceptable for overall situation, which denoted normally less than ±3N control error.

7. Future works

The thruster modeling and control algorithm need to be enhanced in following aspects.

- Near dead-zone region modeling with complementary experiments
- Dead-zone controller

To precise dynamic positioning control of unmanned underwater vehicles, the dead-zone model and control algorithms should be developed.

8. References

Bachmayer, R. & Whitcomb, L. L. (2003). Adaptive parameter identification of an accurate nonlinear dynamical model for marine thrusters, *J. of Dynamic Sys., Meas., and Control,* Vol.125, No.3, 491–494.

Bachmayer, R.; Whitcomb, L. L. & Grosenbaugh, M. A. (2000). An accurate four-quadrant nonlinear dynamical model for marine thrusters: Theory and experimental validation, *IEEE J. Oceanic Eng.,* Vol.25, No.1, 146–159.

Blanke, M.; Lindegaard, K.-P. & Fossen, T. I. (2000). Dynamic model for thrust generation of marine propellers, In: *IFAC Conf. Maneuvering and Control of Marine Craft (MCMC'2000),* pp. 23–25.

Choi, S. K.; Yuh, J. & Takashige, G. Y. (1995). Development of the omnidirectional intelligent navigator. IEEE *Robotics and Automation Magazine,* Vol.2, No.1, 44–53.

Fossen, T. I. & Blanke, M. (2000). Nonlinear output feedback control of underwater vehicle propellers using feedback form estimated axial flow velocity. *IEEE J. Oceanic Eng.,* Vol.25, No.2, 241–255.

Healey, A. J.; Rock, S. M.; Cody, S.; Miles, D. & Brown, J. P. (1995). Toward an improved understanding of thruster dynamics for underwater vehicles. IEEE J. Oceanic Eng., Vol.20, No.4, 354–361.

Manen, J. D. V. & Ossanen, P. V. (1988). *Principles of Naval Architecture, Second Revision, Volume II: Resistance, Propulsion, and Vibration,* Soc. of Naval Architects and Marine Engineers, ISBN, Jersey City, NJ.

Newman, J. N. (1977). *Marine Hydrodynamics,* MIT Press, Cambridge, MA.

Saunders, A. & Nahon, M. (2002). The effect of forward vehicle velocity on through-body AUV tunnel thruster performance. In: *IEEE/MTS OCEANS '02,* pp. 250–259.

Whitcomb, L. L. & Yoerger, D. R. (1999a). Development, comparison, and preliminary experimental validation of nonlinear dynamic thruster models. *IEEE J. Oceanic Eng.,* Vol.24, No.4, 481–494.

Whitcomb, L. L. & Yoerger, D. R. (1999b). Preliminary experiments in model-based thruster control for underwater vehicle positioning. *IEEE J. Oceanic Eng,* Vol. 24, No.4, 495–506.

Yoerger, D. R.; Cooke, J. G. & Slotine, J.-J. E. (1990). The influence of thruster dynamics on underwater vehicle behavior and their incorporation into control system design. *IEEE J. Oceanic Eng,* Vol.15, No.3, 167–178.

Underwater Vehicles

Edited by Alexander V. Inzartsev

ISBN 978-953-7619-49-7
Hard cover, 582 pages
Publisher InTech
Published online 01, January, 2009
Published in print edition January, 2009

For the latest twenty to thirty years, a significant number of AUVs has been created for the solving of wide spectrum of scientific and applied tasks of ocean development and research. For the short time period the AUVs have shown the efficiency at performance of complex search and inspection works and opened a number of new important applications. Initially the information about AUVs had mainly review-advertising character but now more attention is paid to practical achievements, problems and systems technologies. AUVs are losing their prototype status and have become a fully operational, reliable and effective tool and modern multi-purpose AUVs represent the new class of underwater robotic objects with inherent tasks and practical applications, particular features of technology, systems structure and functional properties.

InTech Europe
University Campus STeP Ri
Slavka Krautzeka 83/A
51000 Rijeka, Croatia
Phone: +385 (51) 770 447
Fax: +385 (51) 686 166
www.intechopen.com

InTech China
Unit 405, Office Block, Hotel Equatorial Shanghai
No.65, Yan An Road (West), Shanghai, 200040, China
中国上海市延安西路65号上海国际贵都大饭店办公楼405单元
Phone: +86-21-62489820
Fax: +86-21-62489821

IntechOpen